LAWRENCE
LIVERMORE
NATIONAL
LABORATORY

LLNL-JRNL-768921

# Microstructural Characterization of Pure Tin Produced by the Drop-on-Demand Technique of Liquid Metal Jetting

Y. Idell, N. Watkins, A. Pascall, J. Jeffries, K. Blobaum

March 5, 2019

Scripta Materialia

## Disclaimer

# Microstructural Characterization of Pure Tin Produced by the Drop-on-Demand Technique of Liquid Metal Jetting

Yaakov Idell*, Nicholas Watkins, Andrew Pascall, Jason Jeffries, Kerri Blobaum

Materials Science Division, Lawrence Livermore National Laboratory, Livermore, CA 94550, USA

* Corresponding author; email address: idell1@llnl.gov

Keywords: Additive Manufacturing; EBSD; X-Ray Diffraction; Microstructure

## Abstract

The microstructural-property relationship of a pure tin part built using the drop-on-demand technique of liquid metal jetting, a cost-effective alternative to selective laser melting or sintering techniques, was determined. The microstructure of the as-built tin is observed to have minimal stored strain, low dislocation density, few to no voids, and only the β-tin phase was present; concurrently, mechanical properties are shown to be identical to traditionally manufactured tin.

## Manuscript

In recent years, liquid metal jetting[1] (LMJ), a solid freeform fabrication process for producing 3-D metallic parts through the control of metal droplets, has drawn a considerable amount of interest as a cost-effective alternative to the more prevalent selective laser melting techniques of additive manufacturing. Due to the non-contact direct deposition associated with LMJ, it does not require the need for expensive spherical metal powder feedstock, equipment, or molds. LMJ has already been shown to be important in the electronic manufacturing industry where it can supplant traditional photolithography and plating methods due to reduced manufacturing time, lower cost, and no requirement for acid washes [1,2]. LMJ has two major techniques: uniform droplet spray (LMJ-UDS) and drop-on-demand (LMJ-DoD). The LMJ-UDS technique is based on Rayleigh's capillarity instability of a laminar jet where a jet of molten metal is broken into uniform droplets by applying a periodic perturbation to the jet at a specific frequency and amplitude [3–5]. LMJ-UDS is considered a continuous jetting technique because the formation of droplets occurs at a measurable distance below the nozzle or orifice from where the jet emanates from. This technique can spray metal droplets with great uniformity and high generation rate; however, it can be challenging to control the droplet position for high droplet generation and deposition rate [6]. On the other hand, the LMJ-DoD technique produces discrete droplets at the nozzle by inducing a volumetric change in the fluid either through displacement of a piezoelectric material that is coupled to the fluid [1], a high-speed solenoid to generate the necessary pulse pressure [7–9], or inducing an internal current in the molten metal through an external electromagnetic field [10]. The resulting volumetric change causes pressure and velocity transients to occur in the fluid; thus, this produces a droplet that issues from the nozzle or an orifice [11]. A droplet is created only when it is desired in drop-on-demand mode systems and the droplet size is on the order of the LMJ-DoD nozzle diameter.

Most studies related to LMJ-DoD have been focused on the development of the metal jetting head, analysis of molten metal droplet behavior, or application of the ejected metal droplet; however, very few studies have been conducted in developing the microstructure-property relationship of an as-built LMJ-DoD produced part. The resulting microstructure from the LMJ-DoD process can be complex due to the repeated thermal transients the part experiences during the build process along with a cooling rate that is faster than traditional casting. These differences can lead to the formation of voids, dendrites, unwanted phases, artifacts, and high residual stresses, which likely will lead to differing microstructure-property relationships. During the LMJ-DoD printing process, the droplets are ejected with a velocity that typically ranges from 0.2 m/s to 10 m/s [1] and cool only slightly during flight before impacting the substrate. Upon impact with the substrate, the droplet cools rapidly. The thermal diffusion from the droplet to surrounding materials determines the cooling rate, which can be controlled by modifying the

processing parameters such as the droplet ejection velocity, size, frequency, or substrate temperature. It is important to be able to have control over the solidification of the microstructure in order to attain the optimal mechanical properties for the as-built part. In this study, pure tin was used as a feedstock material to develop an improved understanding of the resultant microstructures from an as-built LMJ-DoD part.

A schematic of the custom-built LMJ-DoD system is shown in Figure 1a. Commercially available 99.95 % tin was placed in the temperature-controlled melt chamber, which was heated and held at 340 °C – well above the melting temperature of tin (232 °C). While the feedstock was melting, the cartesian coordinates to create a 40 mm x 80 mm rectangle "picture frame" were inputted into a custom Matlab program on the experimental control computer. The program controlled the geometry and timing of droplet dispensing as well as droplet frequency and velocity (the latter based on electronically regulated pressure). Once the feedstock was completely melted, the printing script was initiated, and 1 mm droplets of molten tin were dispensed through a 400 µm inner-diameter nozzle using high-speed valves operating at 100 Hz. A valve that controlled pressure actuation was connected to $N_2$ gas that was electronically regulated down to 1 psi (chosen to break the nozzle surface tension, calculated to be 0.8 psi). A second valve was operated at 180□ out of phase from the pressure valve to ensure precise droplet dispensing by preventing chamber over-pressurization. Droplets were deposited onto a stainless-steel substrate controlled by a high-resolution X-Y positioning stage (Figure 1b). Post-analysis showed average droplet velocity of 0.5 m/s.

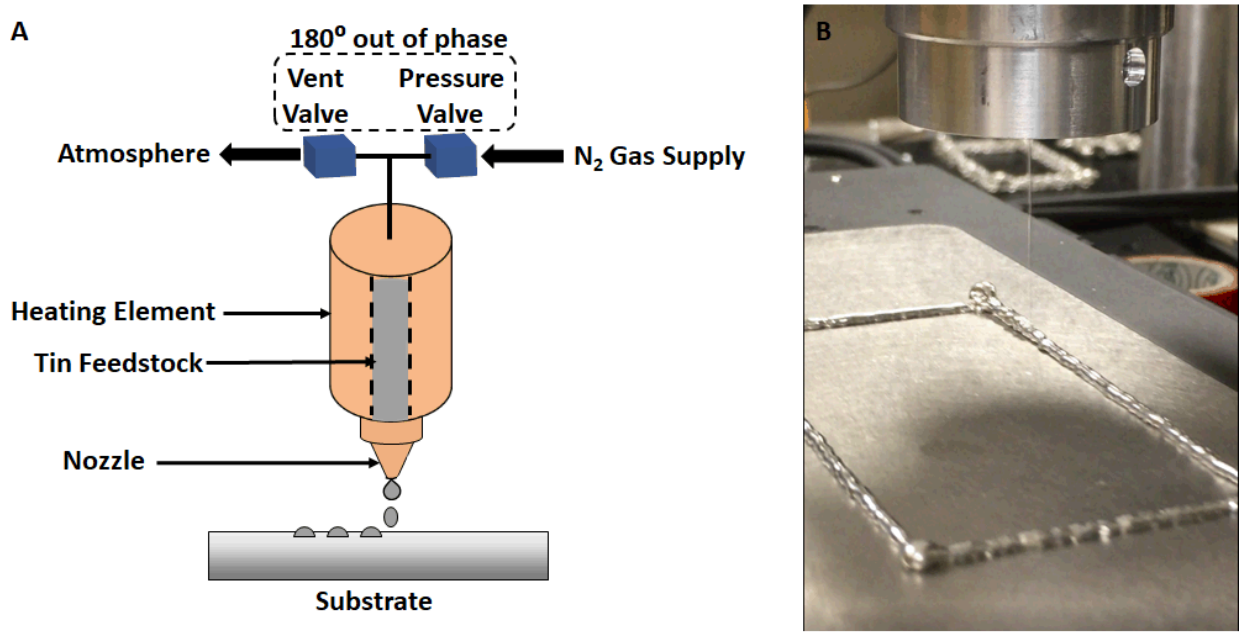


Figure 1: (a) Schematic of the custom-built LMJ-DoD system; (b) the "picture frame" part being built where the tin droplets are being deposited onto a stainless-steel substrate that is controlled by a high-resolution X-Y positioning stage.

The microstructural and property relationships were analyzed through a combination microscopy, roughness, density, and x-ray diffraction (XRD) measurements of the as-built LMJ-DoD part in both the plan-view and cross-sectional view orientations in addition to being compared with the tin feedstock material. The microstructural and property relationships were

characterized using an Ambios Technologies XP-2 stylus surface profilometer, a Phase II 900-391D hardness tester using a load of 50 g and a dwell time of 10 s, a Mettler Toledo PR1203 digital scale with a Mettler Toledo density determination kit using Fluorinert (FC-43) as the density fluid medium, a Bruker D8 Discover X-ray diffractometer operated at 40 kV and 40 mA with copper K-alpha radiation ($\lambda$ = 0.15406 nm) that was fitted with the LYNXEYE detector in a symmetric Bragg–Brentano setup and collected with a 2θ scan range between 30 ° to 90 °, a Keyence VHX-6000 for optical microscopy imaging with the samples etched in a 93 ml methanol, 5 ml $HNO_3$, and 2 ml HCl solution for 30 s to reveal the grain boundaries, and a Phillips XL-30 field emission scanning electron microscope (SEM) operated at 30 kV, which was equipped with the EDAX Digiview Series S electron backscattered diffraction (EBSD) detector, which permits crystallographic mapping. The EBSD data was collected with a step size of 3 μm, and grain boundaries were defined by a misorientation larger than 15° between neighboring measurement points. To reduce the influence of noise in the results, a grain was defined as comprising of at least five points. Because of the observed irregular grain shape, grain size was determined by measuring the major and minor axes of the grain, and then averaging these values together. Unless otherwise specified, all uncertainties in this paper are expressed as 1.96 x σ to deliver a 95 % confidence level of the measured result.

Using a mathematical model based on Newton's cooling law [12], we estimate the cooling for our LMJ-DoD process for pure tin to be between 200 °C/s to 250 °C/s. This cooling rate is faster than traditional casting techniques, but slower than processing techniques using rapid solidification; for comparison, here are previously observed cooling rates: permanent mold casting with 10 °C/s to 20 °C/s [13], direct chill casting with 100 °C/s to 110 °C/s [13], selective laser melting with $10^4$ °C/s to $10^6$ °C/s [14–17], and splat quenching with $10^5$ °C/s to $10^6$ °C/s [18] cooling rates. The LMJ-DoD process can be visualized as a micro-casting technique where the cooling rate is higher than traditional as-cast because the increased surface area of the droplets significantly increases heat transfer of the metal droplet.

| | Feedstock | LMJ-DoD Cross-Section | LMJ-DoD Plan-View |
|---|---|---|---|
| Lattice parameter a (Å) | 5.8319 ± 0.0002 | 5.8318 ± 0.0001 | 5.8314 ± 0.0003 |
| Lattice parameter c (Å) | 3.1820 ± 0.0001 | 3.1813 ± 0.0001 | 3.1812 ± 0.0001 |
| Hardness (VHN) | 7.5 ± 0.6 | 8.2 ± 0.8 | 8.0 ± 0.7 |
| Tensile Strength (MPa) | 25 ± 2.0 | 27 ± 2.6 | 26 ± 2.3 |
| Density (g/cm^3) | 7.32 | 7.31 | 7.31 |
| Ra (nm) | - | ≈ 320 | ≈ 200 |
| Wa (μm) | - | ≈ 200 | > 400 |
| Mean grain size (μm) | 111.05 ± 13.85 | 1818.8 ± 598.70<br>692.10 ± 350.70 | 306.54 ± 13.85 |
| Aspect ratio | 1.04 | 4.11 | 1.18 |

Table 1: Summary of selected microstructural metrics and properties identifying that the LMJ-DoD processing technique produces parts with nearly identical mechanical properties to the feedstock.

The surface of the as-built LMJ-DoD part is observed to have a minimal surface roughness with significant amount of surface waviness (Table 1). The minimal surface roughness

is the result of a relatively moderate temperature gradient between the molten tin droplet and substrate (20 °C vs 232 °C), which minimizes any surface-related artifacts created during solidification; meanwhile, the large surface waviness is a result of the impacted droplets overlapping each other. Figures 2a to 2c compare the etched microstructure of the feedstock material with the plan-view and cross-sectional view orientations of the LMJ-DoD produced part. The feedstock material (Figure 2a) shows a microstructure that has an equiaxed grain shape with an average grain size of 111.05 µm ± 13.85 µm and an aspect ratio of 1.04. The plan-view orientation microstructure of the as-built LMJ-DoD part (Figure 2b) shows large, irregular grains with an average grain size of 306.54 µm ± 13.85 µm and an aspect ratio of 1.18; meanwhile, the cross-sectional view orientation microstructure of the as-built LMJ-DoD part (Figure 2c) has a strongly elongated microstructure orientated along the build direction with a bimodal grain size distribution defined by peaks at 1818.8 µm ± 598.70 µm and 692.10 µm ± 350.70 µm and aspect ratio of 4.11. The elongated grains observed in the cross-sectional view orientation are the result of a high velocity solid-liquid interface causing a moderate undercooling. This undercooling causes the growth direction of the grains to be anti-parallel to the heat flow permitting columnar growth to occur. For each new layer being built, the previous layers will receive heat flow from the layer above it resulting in continued columnar grain growth where voids can form on higher cooling rates [19]. The optical micrographs (Figure 2) show no indication of any voids in either the tin feedstock or as-built LMJ-DoD material; density measurements show that the feedstock tin and LMJ-DoD produced parts have nearly identical density at 7.32 g/cm$^3$ and 7.31 g/cm$^3$ respectively further validating that there are very few to no voids in the microstructure.

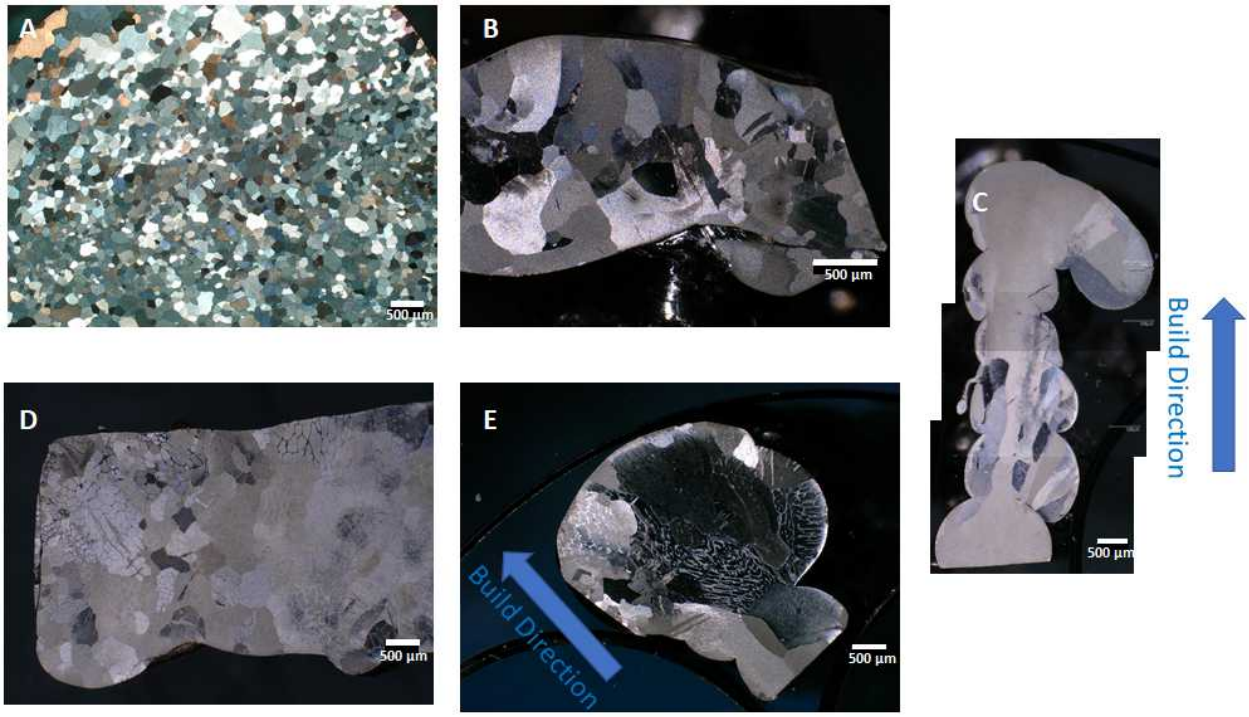


Figure 2: Optical micrographs of the (a) feedstock material, (b) LMJ-DoD of the plan-view orientation, and (c) LMJ-DoD of the cross-sectional view orientation show the large, irregular,

and elongated microstructures formed from the LMJ-DoD process. At the corners of the LMJ-DoD parts, there is a localized pileup area leading to an increased heat flow results in newly recrystallized grains forming in the (d) plan-view and (e) cross-sectional view orientations.

Figure 3 shows the inverse pole figure (IPF) maps collected from EBSD data where the plan-view orientation of the LMJ-DoD part (Figure 3a) reveals several clusters of grains with the same orientation; an example of one such area is shown in Figure 3b. It appears that the initial grain that formed during the solidification of the molten β-tin droplet formed a single large grain. Due to the heat flow from a nearby droplets near the grain, the heat input was enough to initiate recrystallization within this grain transforming the grain shape from a large irregular grain into several grains that have a more equiaxed grain shape. Figures 3c and 3e show a map visualizing the point-to-point misorientation between all neighboring points. This map assumes that any change in orientation within an individual grain must be due to the presence of geometrically necessary dislocations; therefore, the misorientation gradient serves as an approximation of plastic strain [20]. It is clear the microstructure shows a strain-relieved material further validating the heat flow from nearby droplets impacting the microstructural-property relationship. Based on the estimated cooling rate, droplet frequency, droplet size, and scan speeds, it is hypothesized, any thermal strains developed will be relieved by either nearby droplets or the next layer of tin deposition due to the very low recrystallization temperature of pure tin (≈ 30 °C [21]) leading to mechanical properties similar to traditional as-cast tin. The measured hardness validates this hypothesis where hardness values (the related tensile strength values are shown in parenthesis) are 7.5 ± 0.6 VHN (25 ± 2 MPa), 8.2 ± 0.8 VHN (27 ± 3 MPa), and 8.0 ± 0.6 VHN (26 ± 2 MPa) for the tin feedstock, cross-sectional orientation, and plan-view of LMJ-DoD part respectively are measured. These hardness values are consistent with the EBSD data indicating a strain-relieved microstructure with low dislocation density. The LMJ-DoD produced part has very similar hardness values even though it is a strain relieved microstructure with significantly larger grain size. It is hypothesized that the similar hardness is related to the highly anisotropic nature of tin [22]. The anisotropy in tin is strongly influenced by crystal orientation and direction due to the tetragonality of the tin unit cell where a high probability of {110} set of planes can relate to an increase in stiffness resulting in a higher hardness.

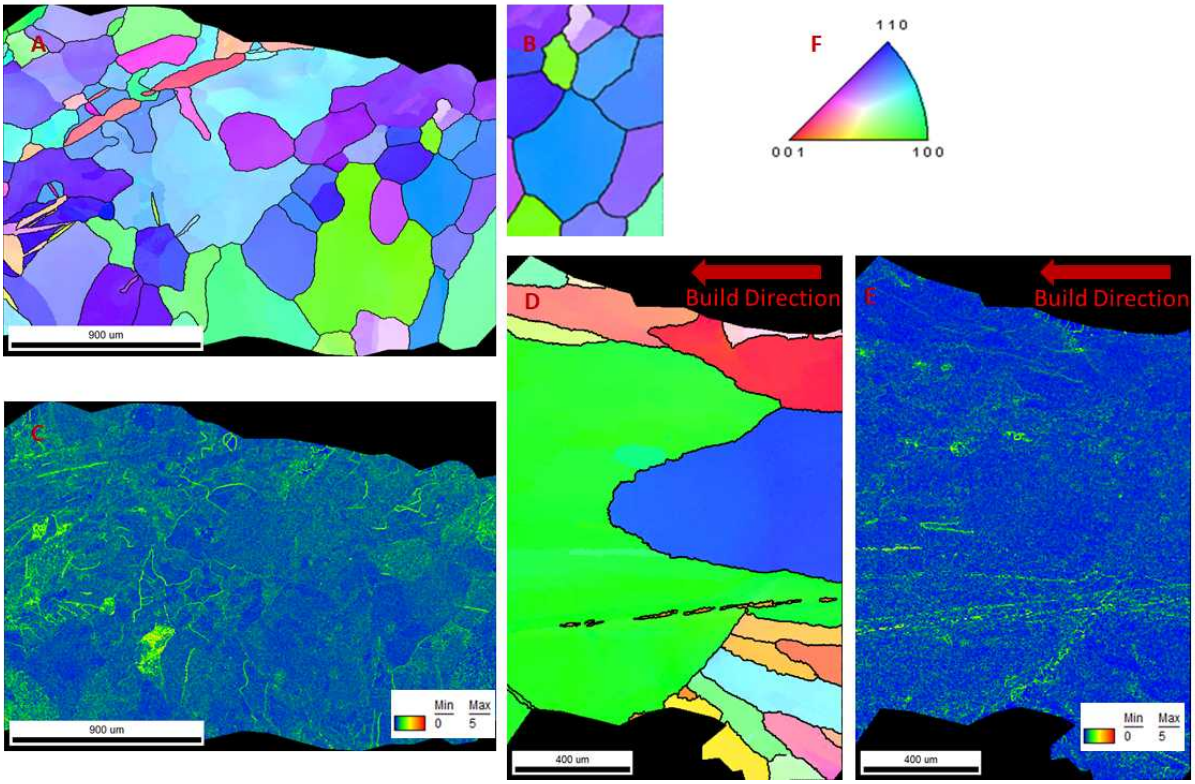


Figure 3: Inverse pole figure (IPF) maps for the LMJ-DoD produced part of the (a) plan-view (the sample direction is normal to the build direction) and (d) cross-sectional (the sample direction is parallel to the build direction) orientations show microstructural grain orientation including (b) clustering of similar grain orientations observed in the plan-view. The local average misorientation maps for the (c) plan-view and (e) cross-sectional view orientations reveal a strain-relieved microstructure with low dislocation density; (f) IPF legend for (a), (b), and (d).

Figure 4 compares the XRD scans of the tin feedstock with the as-built LMJ-DoD tin. The tin feedstock scan shows the signature XRD peak positions and intensity ratios typical for β-tin with high-intensity body centered tetragonal peaks. The LMJ-DoD produced material shows nearly identical XRD scans in both the cross-sectional and plan-view orientations where no significant texture or additional phases are present in the samples. A full Rietveld analysis of the XRD data was conducted using the general structure and analysis system crystallographic package (GSAS-II) [23] fitted with a pseudo-voigt function. The lattice parameters are shown in Table 1. It is shown that there is little change in the lattice parameter, less than 0.1 % reduction in the unit cells from the feedstock to the as-built condition, indicating very little stored strain from the LMJ-DoD build process, which agrees with the hardness and EBSD data. Even though the mechanical properties of the LMJ-DoD produced parts are similar to the tin feedstock, the irregular grain shape may cause unexpected wear resistance or corrosion failure, which have been observed in other transition metals previously [24]. A post-deposition heat treatment may be necessary to tune properties for specific applications to prevent unanticipated failures.

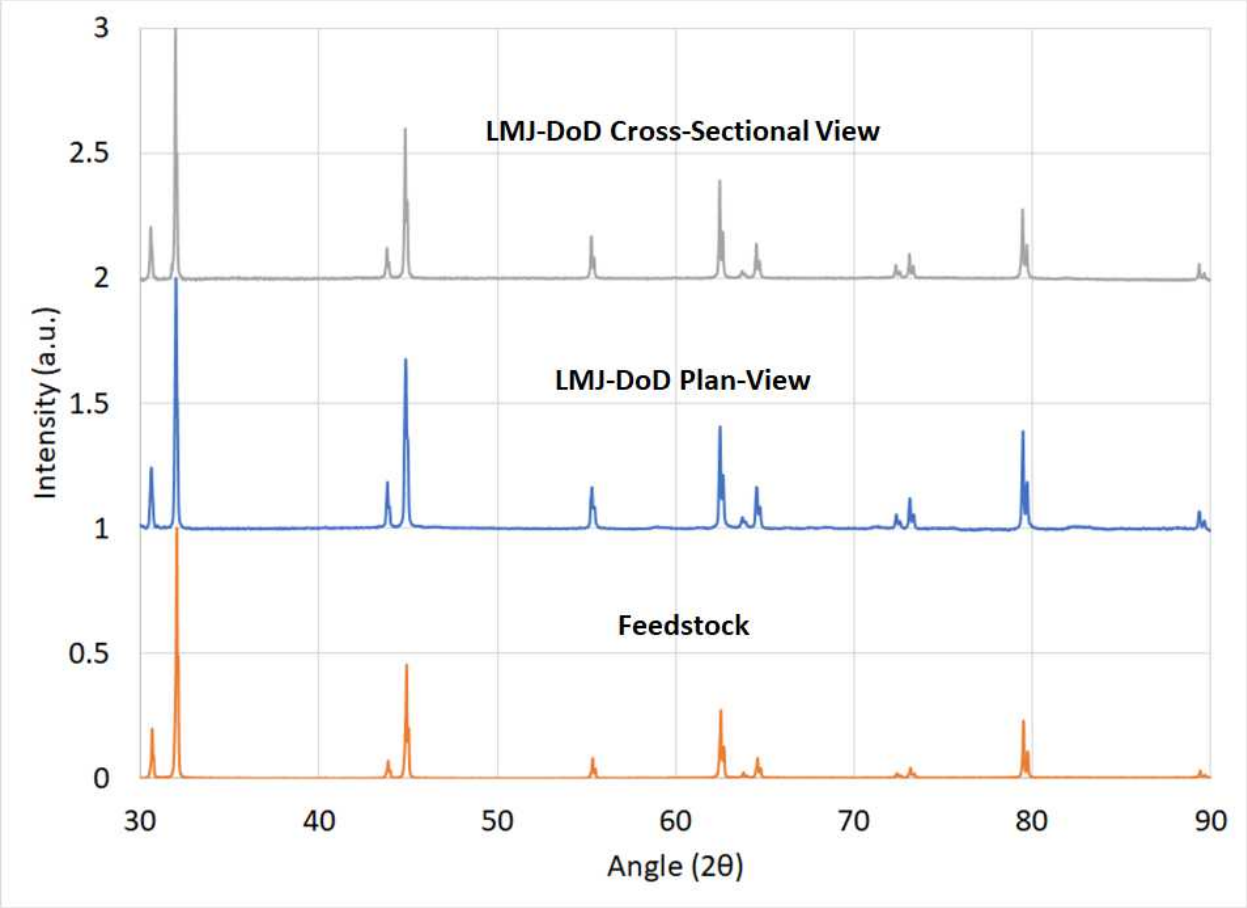

Figure 4 – XRD scans reveal that the LMJ-DoD produced parts are structurally identical to the feedstock where β-tin is the only phase.

It was noted during the LMJ-DoD build process that the tin frame material had a pile-up of material at the corners. This is due to inertia of the positioning stage, which decelerates at the corners leading to a pile-up. The additional material observed at the corners lead to a localized increase in heat flow, which manifested varied microstructure in these areas compared to the straight sections of the part. Figures 2d and 2e show the etched microstructure of the plan-view and cross-sectional views from these localized pile-up areas of the LMJ-built tin. The microstructure of the plan-view orientation (Figure 2d) in the pile-up region shows newly recrystallized grains within the large irregular grains that were observed in the non-pile-up regions with an average grain size of 109.87 µm ± 14.13 µm and an aspect ratio of 1.13, nearly matching the tin feedstock. Meanwhile, the microstructure of the cross-sectional view orientation (Figure 2e) in the pile-up region has newly recrystallized grains with a slightly elongated grain structure orientated along the build direction with an average grain size of 139.65 µm ± 37.65 µm and an aspect ratio of 2.41. The pile-up regions exhibit a microstructure of what would be expected of a partially heat-treated pure metal.

A pure tin 3-D structure can be built through the LMJ-DoD process yielding mechanical properties comparable to tin feedstock produced through traditional manufacturing techniques. The observed microstructure of the as-built LMJ-DoD part displays large, irregular, and

elongated grains orientated along the build direction with minimal stored strain, low dislocation density, few to no voids, and only the β-tin phase. The strain-relieved microstructure is the result of subsequent droplets impacting the surface and providing enough heat input to permit strain relief and even recrystallization at the corners (pile-up areas) of the produced part. A pure tin part made through LMJ-DoD can be viewed as a micro-casting technique that produces mechanical properties identical to traditionally manufactured tin.

This work was performed under the auspices of the U.S. Department of Energy by Lawrence Livermore National Laboratory under Contract DE-AC52-07NA27344 and was supported by the LLNL-LDRD program under project number 18-SI-001. LLNL release number LLNL-JRNL-768921.

## References


1 T.M. Lee, T.G. Kang, J.S. Yang, J. Jo, K.Y. Kim, B.O. Choi, and D.S. Kim: *IEEE Trans. Electron. Packag. Manuf.*, 2008, vol. 31, pp. 202–10.

2 A. Pan, E. Hanson, and M. Lee: *J. Imaging Sci. Technol.*, 2010, vol. 54, pp. 10501–3.

3 Lord Rayleigh: *Proc. London Math. Soc.*, 1878, vol. 1, pp. 4–13.

4 Lord Rayleigh: *London, Edinburgh, Dublin Philos. Mag. J. Sci.*, 1892, vol. 34, pp. 145–54.

5 F. Savart: *Anal. Chem.*, 1833, vol. 53, pp. 337–86.

6 R. Godin: *Nepcon Texas Proceedings, Texas, USA*.

7 S. Cheng and S. Chandra: *Exp. Fluids*, 2003, vol. 34, pp. 755–62.

8 J. Luo, L. Qi, S. Zhong, J. Zhou, and H. Li: *J. Mater. Process. Technol.*, 2012, vol. 212, pp. 2066–73.

9 S. Zhong, L. Qi, J. Luo, H. Zuo, X. Hou, and H. Li: *J. Mater. Process. Technol.*, 2014, vol. 214, pp. 3089–97.

10 Z. Luo, X. Wang, L. Wang, D. Sun, and Z. Li: *Mater. Lett.*, 2017, vol. 188, pp. 184–7.

11 D.B. Wallace: *J. Fluids Eng.*, 1993, vol. 115, pp. 529–32.

12 X. Yi, N. Ellendt, X. Li, V. Uhlenwinkel, and U. Fritsching: *Trans. Nonferrous Met. Soc. China*, 2017, vol. 27, pp. 1636–44.

13 S.W. Xu, K. Oh-ishi, S. Kamado, H. Takahashi, and T. Homma: *Mater. Sci. Eng. A*, 2012, vol. 542, pp. 71–8.

14 D. Herzog, V. Seyda, E. Wycisk, and C. Emmelmann: *Acta Mater.*, 2016, vol. 117, pp. 371–92.

15 J. Suryawanshi, K.G. Prashanth, S. Scudino, J. Eckert, O. Prakash, and U. Ramamurty: *Acta Mater.*, 2016, vol. 115, pp. 285–94.

16 H.Y. Jung, S.J. Choi, K.G. Prashanth, M. Stoica, S. Scudino, S. Yi, U. Kühn, D.H. Kim, K.B. Kim, and J. Eckert: *Mater. Des.*, 2015, vol. 86, pp. 703–8.

17 K.G. Prashanth and J. Eckert: *J. Alloys Compd.*, 2017, vol. 707, pp. 27–34.

18 W. Brower and M. Flemings: *Solidification of Iron Base Alloys at Large Degrees of Undercooling*, 1969.

19 D.G. Morris: *Met. Sci.*, 1982, vol. 16, pp. 457–64.

20 M.F. Ashby: *Philos. Mag.*, 1970, vol. 21, pp. 399–424.

21 R.W. Cahn and P. Haasen: *Physical Metallurgy. Vol. 1*, North-Holland, 1996.

22 T.R. Bieler, H. Jiang, L.P. Lehman, T. Kirkpatrick, E.J. Cotts, and B. Nandagopal: *IEEE*

*Trans. Components Packag. Technol.*, 2008, vol. 31, pp. 370–81.

23 B.H. Toby and R.B. Von Dreele: *J. Appl. Crystallogr.*, 2013, vol. 46, pp. 544–9.

24 K.D. Ralston and N. Birbilis: *Corrosion*, 2010, vol. 66, p. 75005.